

FOURIER TRANSFORM ION CYCLOTRON RESONANCE MASS SPECTROMETRY: THE TEENAGE YEARS

Alan G. Marshall¹ and Peter B. Grosshans

Department of Chemistry
The Ohio State University
120 West 18th Avenue
Columbus, OH 43210

Fourier transform ion cyclotron resonance mass spectrometry (FT-ICRMS or FT-MS) is a technique that effectively converts ionic mass-to-charge ratio, m/q , to an experimentally measurable ion cyclotron orbital frequency, ν_c , given approximately by

$$\nu_c = \frac{qB_0}{2\pi m} \quad (\text{S.I. units}) \quad (1)$$

in which B_0 is the strength of an applied static magnetic field. Because frequency can be measured more accurately than any other physical property (1), FT-ICRMS offers potentially ultrahigh mass measurement accuracy (1 part in 10^9 or better) as well as other advantages that will be discussed later. Note that the chemical formula of an ion may be determined directly from its mass alone, if the mass is measured accurately: for example, N_2^+ at 28.0056 u versus CO^+ at 27.9944 u.

Although ions in a static magnetic field execute circular ICR orbital motion (see Figure 1), simply placing such ions between a pair of detection electrodes will not produce a signal, any more than placing a sample in an FT-NMR spectrometer will spontaneously generate an NMR signal. It is necessary to excite a packet of ions of a given mass-to-charge ratio coherently to larger ICR orbital radius, so that the spatially coherent orbiting ion packet induces an oscillating difference in charge between two opposed detection electrodes. Current will then flow (at the cyclotron frequency) between the detection plates. Forcing that current

to pass through an impedance "converts" the current to a voltage difference between the electrodes. That voltage difference can then be amplified to give a time domain free ion decay signal (see glossary, p. 216 A) that can be digitized and Fourier transformed to yield a frequency domain spectrum. Conversion from the frequency scale to a mass

ICRMS grew rapidly in unforeseen ways, and behavioral flaws that were excusable in an infant soon became unacceptable for an adult. In this article, we describe the adolescent maturation of the FT-ICRMS technique.

The initial enthusiasm and early applications for FT-ICRMS were based on its highly linear behavior: In uni-

INSTRUMENTATION

(actually mass-to-charge ratio) scale may then be performed algebraically from Equation 1 or from more accurate expressions discussed below.

Seventeen years ago (2) the infant FT-ICRMS technique exhibited the same genetic traits that distinguished its FT-IR and FT-NMR spectroscopic forebears: the multiplex (Fellgett) advantages for speed (by a factor up to 10^6) or signal-to-noise ratio (S/N) (factor of up to 10^3) compared with its single-channel ICR parent technique, as well as the unique advantage of potentially ultrahigh resolving power. As with any promising youngster, FT-

form magnetic (and no electric) field, m/q is linearly related to the observed ICR orbital frequency, ν_c (in Hz), according to Equation 1, and the detected FT-ICR signal (i.e., differential voltage induced between two infinite parallel electrodes) is directly proportional both to the number of ions of a given m/q value and to their cyclotron orbital radius.

For on-resonance single-frequency excitation between infinite parallel electrodes, the postexcitation cyclotron orbital radius of an ion is proportional to the product of the radiofrequency (rf) excitation voltage magni-

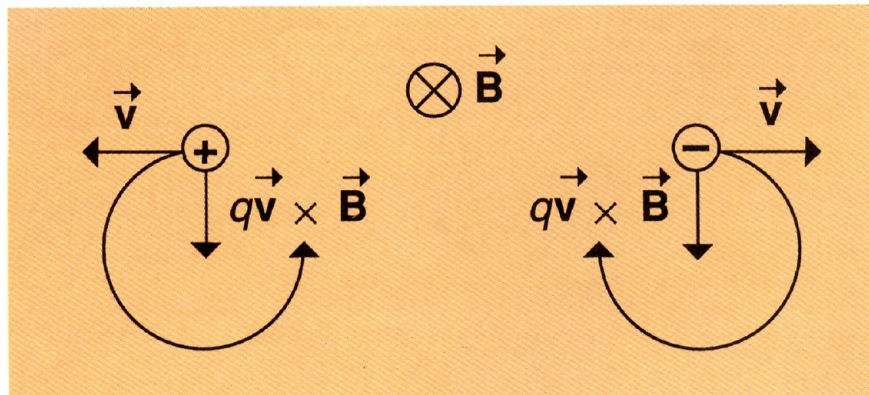


Figure 1. Magnetic force acting on a positive (left) and negative (right) ion, each with velocity, \mathbf{v} , subjected to a static magnetic field, \mathbf{B} , directed into the plane of the paper.

Note the opposite sense of rotation for ions of opposite charge, because changing the sign of q in Equation 2 ($\mathbf{F} = q\mathbf{v} \times \mathbf{B}$) changes the sign (and thus the direction) of the Lorentz magnetic force.

¹ Also a member of the Department of Biochemistry.

tude and duration (3). In this idealized case, the mass-to-charge ratio of ions of any m/q value could be determined with ultrahigh precision simply by determining B_0 from the FT-ICR spectral frequency, ν_c , for ions of a single known m/q value. Moreover, the observed relative FT spectral magnitudes at various ν_c values would directly reflect the relative numbers of ions of corresponding m/q values.

However, as we shall see, an actual

FT-ICR experiment requires that ions be confined ("trapped") within a finite volume bounded by conductive electrodes (which may be plates, screens, rods, or wires). Those electrodes necessarily produce spatially warped static and rf electric fields in the ion trap with several generally undesirable consequences. First, the relation between ICR orbital frequency and m/q becomes nonlinear, making mass calibration more difficult (4–8). Second, ICR

signal strength no longer varies linearly with rf excitation magnitude and duration (9, 10) or even ICR orbital radius (9, 11, 12), and (even worse) some of these nonlinearities are mass dependent. Third, coulomb forces between ions broaden and shift the mass spectral peaks (6, 13, 14). Finally, the spatially nonuniform excitation field may even eject ions axially before they can be detected (15–19).

Although a full analytical solution

Glossary

- Broadband:** Simultaneous transmission or detection covering a wide range of frequencies
- Burst excitation** (see also impulse excitation): A shaped brief rf waveform whose frequency domain spectrum covers a wide range centered at the excitation frequency
- Critical mass:** Ion mass above which ions cannot be trapped in stable ICR orbits (see Equation 7)
- Cyclotron motion:** Rotation of an ion about a fixed applied magnetic field (see Figure 7)
- Daughter ions:** Ions formed by nonreactive or reactive ion-neutral collisions
- Differential charge, ΔQ :** Charge induced on one detector electrode minus the charge induced on an opposed detector electrode
- Differential voltage, ΔV :** Voltage difference between two opposed detector (or transmitter) electrodes, usually connected through an impedance
- Direct-mode ICR detection:** Amplification and analog-to-digital conversion of the signal obtained directly from the differential voltage induced between the detector electrodes
- Fellgett advantage:** The advantage in speed (for a given resolution) or S/N (for a given total data acquisition period) gained by simultaneous detection of the whole spectrum rather than single-channel scanning of one spectral element at a time. For an N -point spectrum, the Fellgett speed advantage is a factor of N and the S/N advantage is \sqrt{N}
- Free ion decay:** Time domain ICR signal (by analogy to free-induction decay in magnetic resonance)
- Frequency domain spectrum:** Spectrum obtained by Fourier transformation of a time domain signal
- Frequency sweep (chirp) excitation:** Excitation waveform in which frequency varies linearly with time over a period that is short compared with the damping constant for exponential disappearance of the time domain ICR signal
- Hadamard transform:** A particular algorithm for encodement and decodement corresponding to simultaneous detection of the daughter ions of approximately half of the parent ions of interest
- Harmonic frequency:** An integral multiple of the fundamental frequency; the fundamental frequency is also known as the first harmonic frequency
- Heterodyne mode ICR detection:** As in direct mode, except that the detected differential voltage is amplified and multiplied by the output from a fixed ("carrier") frequency oscillator and low-pass-filtered to yield a relatively narrowband signal
- Impulse excitation:** dc excitation in such a short period that signals spanning effectively all of the spectral range of interest are excited simultaneously
- Magnetron motion:** Slow (typically a few hundred Hz) circular drift of an ion along a path of constant electrostatic potential (see Figure 7); magnetron motion occurs as a result of the crossed radial electric field and axial magnetic field
- Mass calibration:** In ICR, conversion of observed ICR spectral frequencies to accurate mass-to-charge ratios (see Equation 8)
- Mass resolving power:** $m/\Delta m$, in which m is ionic mass and Δm is the width of the mass peak (typically taken as the full width at half-maximum FT-ICR mass spectral peak height). Δm is also known as the mass resolution
- Modulation:** Variation (often sinusoidal) of one observable resulting from oscillation of some other quantity (e.g., variation in ICR orbital frequency, ν_c , because of trapping oscillation of ions between regions of different electric or magnetic field strength). The amplitude (AM) and/or frequency (FM) may be modulated
- MS/MS:** Mass spectrometry/mass spectrometry, in which the first stage of mass separation is designed to select parent ions of a given mass-to-charge ratio, and the second stage is designed to detect all of the daughter ions resulting from fragmentation or ion-molecule reaction of the initially selected parent ions
- Narrowband:** Transmission or detection covering a narrow range of frequencies
- Parametric excitation and detection:** In a hyperbolic ion trap, application or detection of the voltage between the (unbroken) ring electrode and the end cap electrodes
- Parent ions:** Ions selected in the first stage of an MS/MS experiment
- Penning ion trap:** A hyperbolic ion trap operating in an axial magnetic field
- Quadrature:** Used to denote either the second channel in a two-channel quadrature experiment or an experiment in which both the unshifted and 90° phase-shifted quadrature components of a signal are transmitted or detected simultaneously
- Quadrupolar potential:** Defined in Equation 6, it approximates the actual electrostatic potential near the center of an ICR ion trap and may be generated exactly by a hyperbolic trap (see p. 224 A)
- Radial ejection:** Excitation of ion cyclotron orbital motion to an ICR orbital radius larger than the transverse boundary of the ion trap
- Reciprocity:** The principle that relates the electric potential at a field point within an ion trap when a potential is applied to a detector electrode to the charge induced on that electrode by a unit charge placed at the same position (see p. 225 A)
- Resonance:** The condition in which the excitation frequency is the same as a natural frequency (e.g., cyclotron, magnetron, trapping, or combinations or multiples thereof) of the system
- Sidebands:** Signals (usually of reduced magnitude) that appear at equally spaced intervals above or below the fundamental frequency (see p. 223 A)
- Solenoidal supercon magnet:** A magnet constructed with superconducting wire wound around a cylinder so as to produce a strong magnetic field along the central axis
- Spatial coherence:** Ions bunched in a packet whose dimensions are much less than the ICR orbital radius
- SWIFT:** Stored waveform inverse Fourier transform, a means for generating an arbitrary excitation waveform for mass-selective excitation or ejection of ions (see p. 220 A)
- Time domain ICR signal:** Detected differential voltage between the ICR detector electrodes
- Trapping oscillation:** Axial back-and-forth motion of ions trapped between two plates to which a positive dc potential, relative to the field, has been applied
- Two-dimensional ICR:** Hadamard or Fourier methods for extending the Fellgett advantage to the first stage (i.e., parent ion selection) of an MS/MS experiment
- z-ejection:** Excitation of ion-trapping oscillation to an amplitude exceeding the z-boundary of the trap

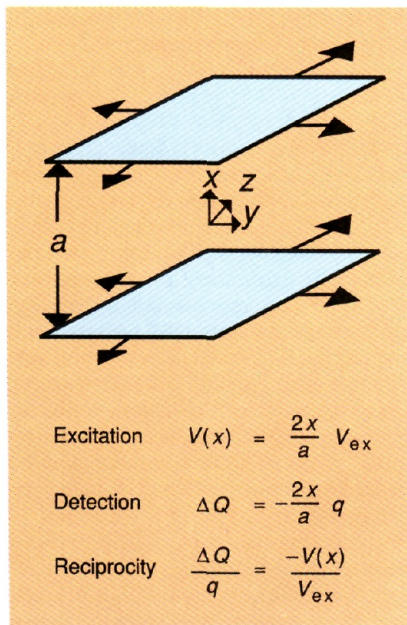


Figure 2. The reciprocity principle, demonstrated for infinitely extended parallel planar electrodes located at $x = \pm a/2$.

If a potential V_{ex} is applied to the upper electrode and $-V_{ex}$ to the lower electrode, the potential anywhere between the electrodes is $V_{ex}(2x/a)$. By symmetry, the potential cannot depend on y or z ; thus, only a linear function of x can satisfy Laplace's equation, $\nabla^2 V = 0$. Alternatively, if a point charge, q , is located somewhere between the electrodes, it can be shown that the difference, ΔQ , between the charge induced on the upper and lower electrodes is $-q(2x/a)$. The relationship, $\Delta Q/q = -V/V_{ex}$, illustrated here for infinitely extended electrodes, holds in general; we denote this relation as reciprocity.

for ion behavior in an electromagnetic ion trap is not feasible, most of the critical features of the problem may be understood from simplified models. We therefore begin with a brief review of ion cyclotron orbital motion in a uniform magnetic (and no electric) field, and then show how addition of a spatially uniform rf electric excitation field produced from two infinitely extended parallel electrodes generates an observable ICR signal at the frequency given by Equation 1.

The basis for optimal selection (by stored waveform inverse FT, or SWIFT, excitation) of ions of one or more m/q values is presented, along with two general approaches (Hadamard and Fourier) to two-dimensional (2D) experiments designed for MS/MS applications. Next, we show how the confinement of the ions in a finite electromagnetic box shifts the ICR orbital frequency and introduces two new kinds of natural motions (trapping and magnetron). Finally, we show how the placement of (and interconnections be-

tween) various electrodes affect the magnitude, frequency, and linearity of the detected signal(s), and how the inherent nonlinearity may be eliminated or exploited.

Linear ICR behavior

ICR orbital frequency, resolving power, radius and energy, and upper mass limit. At first glance, any attempt to describe the motion of as many as a million ions subjected to static magnetic as well as static and time-varying electric fields might appear dauntingly difficult. Fortunately, it can be shown that the center-of-mass motion of an ion packet (spatially coherent or not) is unaffected by ion-ion coulomb forces, provided that the applied magnetic field is spatially uniform, the applied electric field varies at most linearly with position, and no other species are present (20). These conditions are satisfied for the idealized case of ions of a given m/q in the region between two infinite parallel electrodes with an applied, uniform magnetic field.

Let the coordinate normal to the electrodes be x (see Figure 2); by sym-

metry, in the absence of ions, the electric potential between the electrodes cannot depend on y or z . For the potential field, V , to satisfy Laplace's equation ($\nabla^2 V = 0$), the potential must be a linear function of x ; that is, the applied electric field is spatially uniform (i.e., $E_x = -\partial V/\partial x = \text{constant}$).

Moreover, if the ions of a given m/q are spatially coherent (i.e., the ions are bunched in a packet whose dimensions are small compared with the ICR orbital radius—see below), then the signal from N ions is simply N times as large as the signal from one ion. In other words, under the stated conditions, the behavior of N identical ions can be understood simply from the behavior of a single ion. Therefore, we begin our description of ion cyclotron motion with a single ion moving under the influence of a spatially uniform magnetic field in the region between two infinite parallel electrodes (i.e., spatially uniform electric field).

The Lorentz force acting on an ion of mass, m , and charge, q , moving at velocity, v , and subjected to an electric field, E , and a static magnetic field, B_0 , is given by

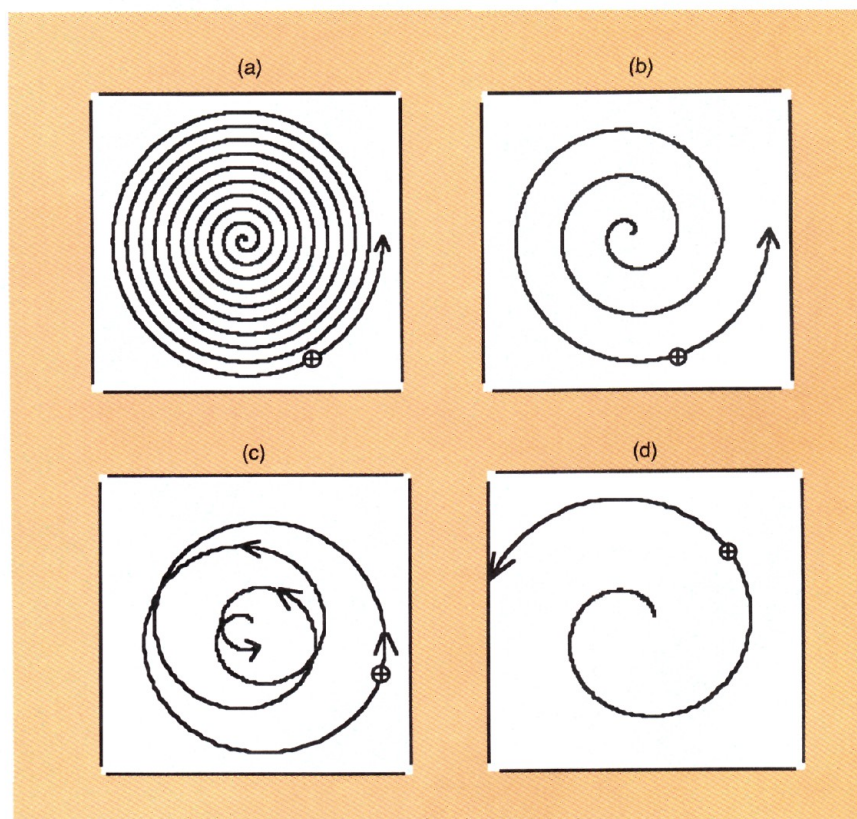


Figure 3. Effects of various ion excitation schemes.

(a, b) Archimedes spirals for ions of two different m/q values excited on resonance for the same length of time at the same excitation voltage magnitude. The ion of lower m/q has the higher cyclotron frequency. (c) Off-resonance excitation resulting in only a small absorption of energy. To make the ion trajectory visible, the scale of this diagram has been greatly enlarged compared with those of the other diagrams in this figure. (d) Ion ejection resulting from high-amplitude resonant excitation.

$$m \frac{d^2\mathbf{r}}{dt^2} = m \frac{d\mathbf{v}}{dt} = q\mathbf{E} + q\mathbf{v} \times \mathbf{B}_0 \quad (2)$$

in which \mathbf{r} is the vector position of the ion and t is time. Let $\mathbf{B}_0 = B_0\mathbf{k}$. The z -axis points along the direction of the magnetic field whose magnitude, B_0 , is constant. In the absence of an electric field, ($\mathbf{E} = 0$), Equation 2 is independent of ion position. An ion moving with speed, \mathbf{v} , in a plane perpendicular to \mathbf{B}_0 will be bent into a circular (ion cyclotron) orbit by the magnetic force that is always directed perpendicular to both \mathbf{B}_0 and the ion velocity vector (Figure 1); because there are no forces acting in the z -direction, the axial (z) motion is unrestrained. Equation 1 then follows immediately from Equation 2, in which ion cyclotron angular velocity, $2\pi\nu_c = \omega_c = v/r$, where r is the radius of the ion cyclotron orbit. ICR frequencies at $B_0 = 3$ T fall within the range $5 \text{ MHz} \geq \nu_c \geq 5 \text{ kHz}$ for singly charged ions of $10 \text{ u} \leq m \leq 10000 \text{ u}$.

Apart from its fundamental connection between m/q and ν_c , Equation 1 has several other immediately useful consequences. First, by taking the differential of Equation 1, we quickly find that mass (or mass-to-charge ratio) re-

solving power, $m/\Delta m$, is the same as frequency resolving power, $\nu_c/\Delta\nu_c$

$$\frac{m}{\Delta m} = \frac{\nu_c}{\Delta\nu_c} \quad (3)$$

in which Δm is the width (say, at half-maximum peak height) of an ICR mass spectral peak and $\Delta\nu_c$ is the corresponding frequency domain peak width (21). In the high-pressure limit (i.e., data acquired for several damping periods of the time domain signal), $\Delta\nu_c$ is directly related to the ion-neutral collision frequency, which is not a strong function of m/q ; thus, Equations 1 and 3 may be combined to show that ICR mass resolving power varies approximately inversely with m/q . Nevertheless, FT-ICR mass resolving power as high as $\sim 10^6$ has been attained at $m/z \approx 900 \text{ u/e}$, where e is the charge of an electron (22), and more than 10^8 at $m/z = 40 \text{ u/e}$ (23).

Second, Equation 1 can be rearranged to yield the ion cyclotron orbital radius, r , if the transverse component of the velocity is known:

$$r = \frac{mv}{qB_0} \text{ in general,} \quad (4a)$$

or $r = (2mkT/q^2B_0^2)^{1/2}$ for an ion of thermal root mean square speed

$$v = (2kT/m)^{1/2} \quad (4b)$$

in which k is the Boltzmann constant and T is temperature (in K). From Equation 4b, one finds that room-temperature singly charged ions of typical mass, $15 \text{ u} < m < 1000 \text{ u}$, have preexcitation ICR orbital radii $< 0.25 \text{ mm}$ at $B_0 = 3.0 \text{ T}$ (i.e., much smaller than the maximum radius allowed by a typical ion trap [10–25-mm radius]). Moreover, a singly charged ion of 100 u excited to an ion cyclotron orbital radius of $\sim 1 \text{ cm}$ at $B_0 = 3.0 \text{ T}$ possesses a translational energy of 434 eV and can generally be induced to fragment on collision with neutral atoms or molecules.

Finally, because $r \propto \sqrt{m}$ in Equation 4b, it is clear that ions of sufficiently high m/q will have thermal ICR orbital radii large enough that some of these ions will collide with one of the trap electrodes. For example, at 300 K and 3 T , an ion of average thermal speed will have an ICR orbital diameter $> 1 \text{ in.}$ when the ion mass exceeds 2700000 u . From the Boltzmann or some other velocity distribution, one could calcu-



The Standard.

late the fraction of ions lost in such a case. In addition, for finite dimension ion traps, there is a "critical" upper mass limit above which ions of even zero initial velocity cannot be trapped.

Excitation and detection of an ICR signal with infinitely extended electrodes. Figure 2 shows the electrostatic potential produced by applying a differential voltage, $\Delta V = 2V_{ex}$, across two infinitely extended flat conductive parallel plate electrodes. Note that the potential varies linearly with distance from either plate. Because force is the negative gradient of potential, the electric force, $F = qE$, on an ion of charge, q , will be independent of ion position between the plates.

Next, let the applied differential voltage oscillate at the ICR orbital frequency $V_{ex} = V_0 \cos(\omega_c t)$ (i.e., linearly polarized resonant excitation). Generally, in FT-ICR, electric field calculations are performed as if the problem were an electrostatic one. That approximation is excellent provided that the wavelength associated with the highest cyclotron frequency of interest is much larger than the trap's dimensions, as is always the case in practice.

The spatially uniform time-varying

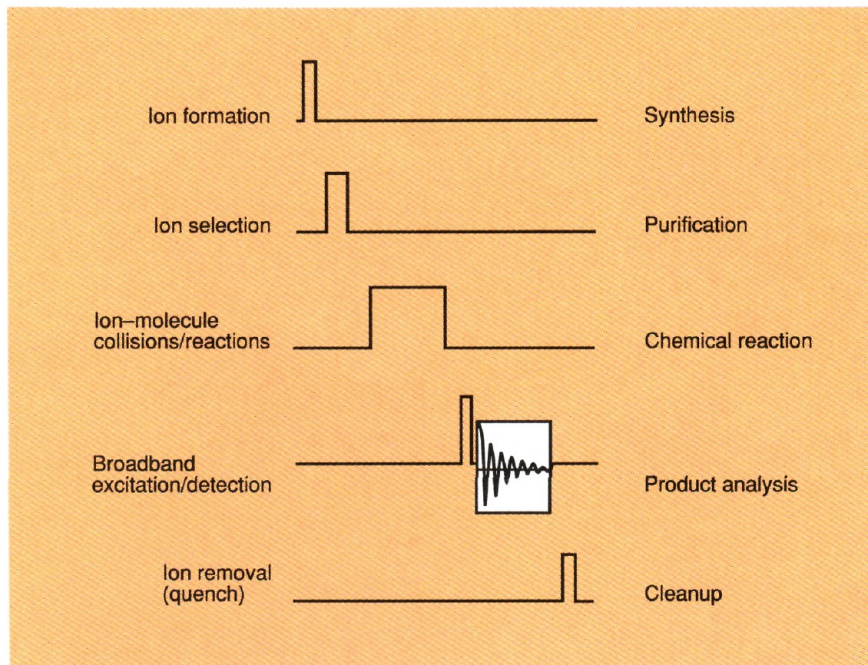
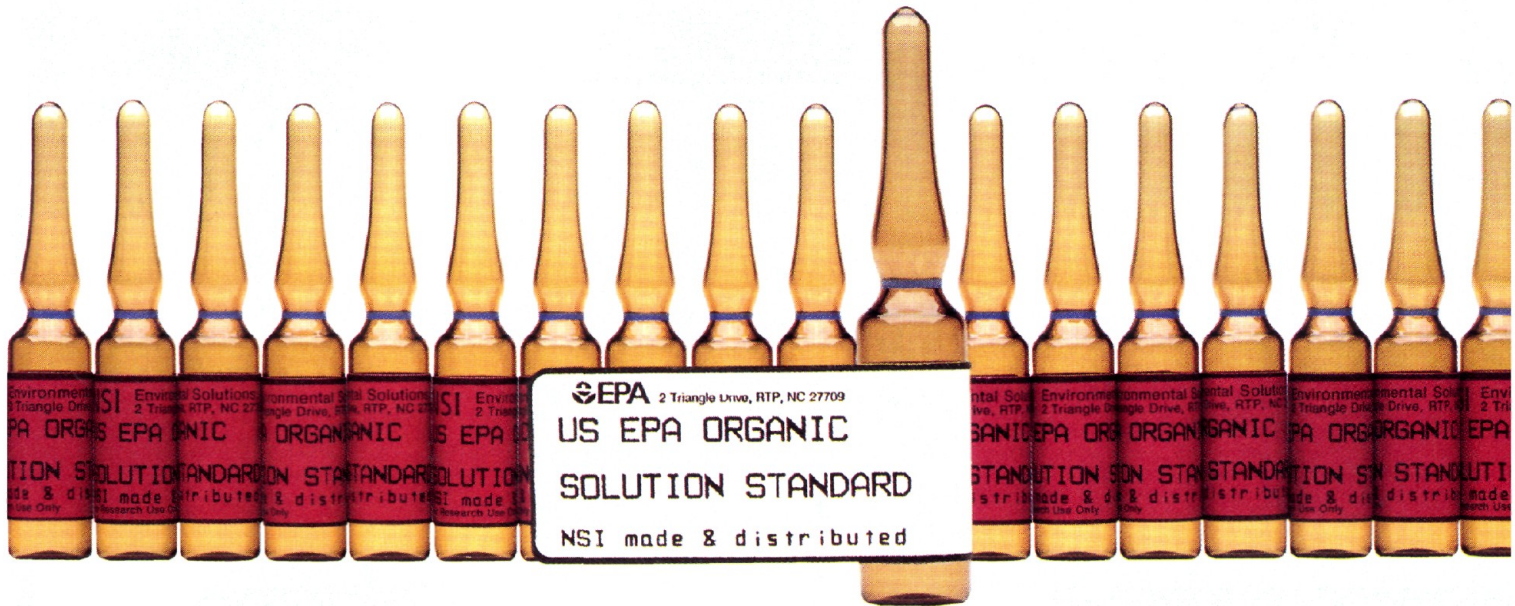


Figure 4. Generalized FT-ICRMS event sequence (left), labeled by the corresponding conventional chemical manipulations (right).

Ions of many m/q values are formed initially. One or more of these parent species may be isolated for subsequent chemical reaction or fragmentation. The parent ions and any daughter ions formed during the reaction period are then mass analyzed. Finally, all ions are swept out of the trap by applying a large potential difference between the trapping plates. (Adapted with permission from Reference 26.)



EPA-Certified Standards From NSI.

Developed in partnership with the EPA and backed by more than a decade of experience, NSI environmental standards are the ONLY EPA-certified organic solutions standards available. NSI and EPA quality-assured, 400 high concentration standards are now available in unlimited quantities—at competitive prices. Order direct from NSI or an NSI authorized distributor.

When reliability is critical, use the EPA-certified standard. Only from NSI. The Environmental Solution.



NSI Environmental Solutions, Inc. • P.O. Box 12313 • Research Triangle Park, NC 27709

Call for free catalog: 1-800-234-7837 (STDS)

CIRCLE 98 ON READER SERVICE CARD

electric field, E , between the plates may be analyzed into two counter-rotating (circularly polarized) components: $E = (V_0/a) \exp(+i2\pi\nu_c t) + (V_0/a) \exp(-i2\pi\nu_c t)$, where a is the plate separation (see Figure 2). The second component rotates in the same sense as the ions and the other in the opposite sense (for positive ions and a right-handed coordinate system).

It can be shown that the ion is significantly affected only by the electric field component rotating in the same sense as the ion. That rotating electric field component acts as a constant force on the ion, pushing it continuously forward in its ICR orbit. Therefore, for an ion initially at rest, the resultant ion trajectory is an Archimedes spiral (Figures 3a and 3b). For ions not initially at rest, the ion trajectories are slightly more complex in the lab frame. However, in a coordinate frame rotating at the ICR frequency they become much simpler (24), just as NMR magnetic moment trajectories are more simply represented in a coordinate frame rotating at the Larmor frequency.

It turns out that ions of different m/q are excited to the same ICR orbital radius when irradiated by resonant ($\nu = \nu_c$) rf electric fields of the same magnitude for the same amount of time. This fortunate property allows us to excite ions having a whole range of m/q values simply by irradiating them with "flat" rf power. The frequency domain spectrum of the excitation signal is constant over the frequencies of interest. Finally, ions subjected to off-resonance irradiation ($\nu \neq \nu_c$) undergo a forced oscillation (24) in ICR radius (Figure 3c; note expanded scale), rather than the continuous increase in ICR orbital radius produced by resonant excitation.

One purpose of an excitation event is to produce a spatially localized ion "packet" in preparation for the detection event. Figure 2 also shows the differential charge, ΔQ , induced between two infinitely extended flat parallel conductive electrodes by an ion of charge, q . In the limit that the ion is infinitesimally close to the upper electrode, a charge of $-q$ is induced on it. Midway between the electrodes ($x = 0$ in Figure 2), the difference in induced charge between the electrodes is zero.

It can be shown that ΔQ is a linear function of the transverse coordinate, x ; thus ΔQ increases linearly with ICR orbital radius (25). Later we will discuss the similarity or reciprocity between ΔV and ΔQ that is exemplified in Figure 2. The unamplified ICR "signal" is the voltage difference produced by the oscillating differentially induced charge across an RC network

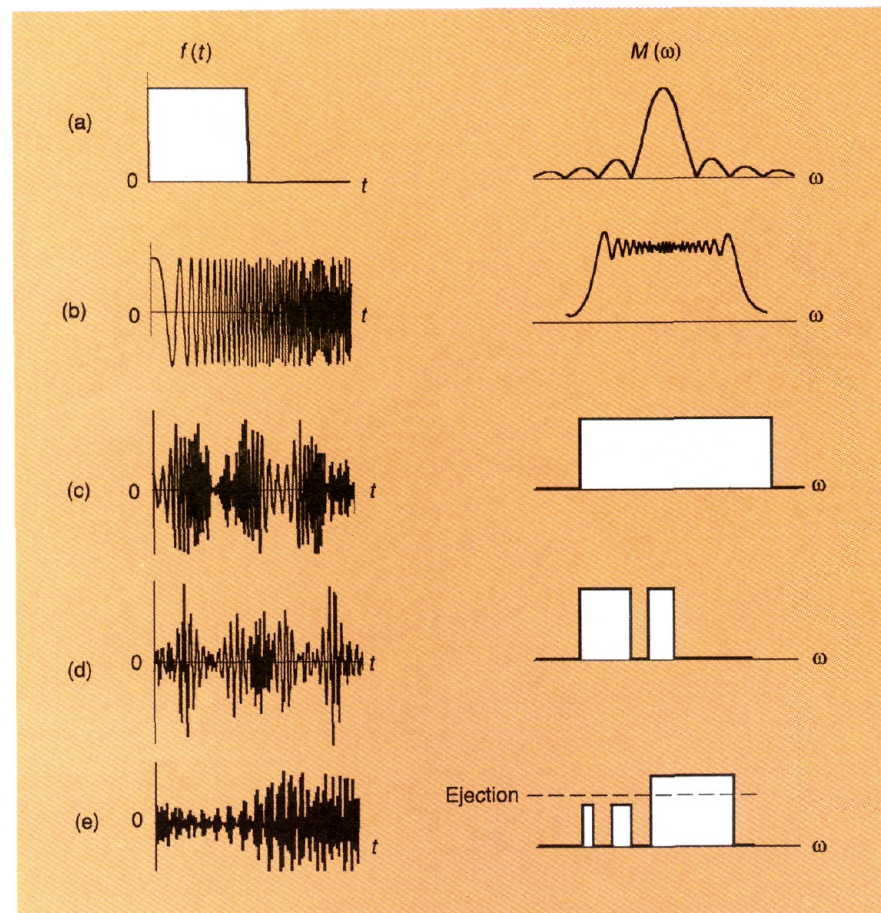


Figure 5. Frequency domain magnitude mode spectra (right) of several FT-ICRMS time domain excitation waveforms (left).

(a) Rectangular pulse excitation waveform. The shorter the duration of the pulse, the more broadband the excitation. (b) Frequency sweep ("chirp") excitation results in a more or less constant frequency domain magnitude over the swept range of frequencies. (c) SWIFT excitation to produce a truly flat frequency domain spectrum over an arbitrary frequency range. (d) SWIFT excitation to produce constant-magnitude excitation over two nonadjacent frequency ranges. (e) SWIFT excitation designed to eject ions within one frequency range and (simultaneously) to excite with equal magnitude ions within either of two other frequency ranges. Note the high uniformity and high selectivity offered by SWIFT excitation and/or ejection in c–e.

connecting the two plates. By design, the ICR signal is essentially independent of frequency, at least for small to moderate m/q values, because the circuit is predominantly capacitive reactive, so that two ions of different m/q with the same trajectory will produce the same ICR signal amplitude.

Excitation of an ICR signal: Impulse, frequency sweep, and SWIFT. Resonant excitation may be exploited in two ways. First, ions may be ejected by exciting them to an ICR orbital radius at which the ions strike the boundary electrodes and are removed (Figure 3d). Alternatively, if ions are excited to a radius ~ 1 cm and the rf voltage is then turned off, each packet of ions of a given m/q value will persist in circular orbit until collisions with neutrals and/or field inhomogeneities disperse the ions (in ICR orbital radius, phase angle, and orbit center) and they no longer form a coherent

packet. During this randomization process, the ions are detected. The basic FT-ICR experimental event sequence (Figure 4; Reference 26) is based on combinations of ion formation, ejection (to select ions of one or more m/q values by ejecting ions of other m/q values), excitation, and detection.

One of the advantages of FT-ICRMS is the ability to simultaneously (or nearly so) excite a wide mass range; obviously, a single-frequency excitation waveform is not well suited for this purpose. Thus we must consider the effects of other waveforms on ions of a given m/q . For the infinite electrode limit (Figure 2), the ICR signal magnitude is proportional to the rf electric field excitation magnitude (i.e., the system is linear), and we need not compute the actual ion trajectory to predict an ion's response to a given excitation waveform. We may simply use a Fourier transform to determine the frequen-

cy domain spectrum of the time domain excitation waveform itself.

Figure 5 shows the effect (i.e., frequency domain magnitude spectrum) of three such waveforms that are capable of producing broadband excitation: a rectangular pulse ("impulse" [2, 27, 28; Figure 5a]), frequency sweep ("chirp" [29, 30; Figure 5b]), and SWIFT (31, 32; Figure 5c–5e). The chirp waveform requires vastly less (factor of 1–1000) excitation voltage magnitude than the impulse function and has until recently been the excitation method of choice in virtually all of the approximately 110 FT-ICR mass spectrometers in use worldwide.

Although both the rectangular pulse and the chirp waveforms can excite ions over a wide m/q range, the excitation magnitude envelope is far from flat over most of the frequency range and is not optimally selective (i.e., broad "shoulders" at each end of the irradiated frequency range). In 1985 we showed that because Fourier transforms work in reverse (i.e., from frequency to time domain) as well as forward (from time to frequency domain), one can specify almost any desired excitation magnitude spectral profile as a discrete magnitude spectrum, and then inverse Fourier transform that data to produce the corresponding time domain excitation waveform. The resulting SWIFT excitation provides optimally flat and selective excitation (Figures 5c and 5d) and/or ejection (Figure 5e) for FT-ICRMS and is now the method of choice for ion selection and excitation in the FT-ICR experimental event sequence of Figure 4. Approximately one-fifth of the FT-ICR mass spectrometers worldwide should be equipped with SWIFT capability by the end of this year.

One- and two-dimensional MS/MS: Hadamard versus Fourier. FT-ICR is uniquely suited for high-resolution multiple-stage MS because the analyte ions remain in the ion trap throughout the experiment. A one-dimensional MS/MS experiment might proceed as follows. Parent ions of all but a chosen m/q value are ejected and then the remaining ions are excited to higher ICR orbital radius and thus higher translational velocity. During a variable delay period, the mass-selected parent ions collide with neutrals and fragment to form daughter ions. Subsequent broadband excitation and detection of the daughter ions yield a high-resolution mass spectrum from which one may reconstruct part or all of the parent ion structure from the chemical formulae of its daughter fragments.

Alternatively, ions of a given m/q value may be isolated and then allowed

to react (rather than fragment) with neutrals to establish ion–molecule reaction pathways, kinetics, energetics, and equilibria, as described in various recent reviews (32–49). For example, we recently used SWIFT excitation and ejection to establish the structures of several osmium cluster ions, Os_n^+ , based on the kinetics of their condensation reactions with their corresponding neutral clusters (50). Multiple-stage MS^n experiments have been used to sort out even more complex ion–molecule reaction pathways (see, e.g., Reference 39).

Although FT-ICRMS offers the multiplex advantage that all of the daughter ions are detected simultaneously in an MS/MS experiment, an obvious disadvantage is that parent ions of all but one m/q are discarded at the outset. Two recent innovations have made it possible to include either half or all of the parent ions simultaneously in 2D MS/MS experiments.

In Hadamard 2D ICR (51), SWIFT

excitation is used to eject a linear combination of approximately half of the N possible parent ions; the remaining parent ions are then excited and allowed to fragment by ion–neutral collisions, and all of the resulting daughters are excited and detected afterward. The process is then repeated for N linearly independent combinations of selected parent ions. (The Hadamard code [26] simply specifies how to choose the various parent ion combinations and how to decode the resulting mass spectra afterward to extract the daughter ion spectrum corresponding to each of the individual parent ions.) Because approximately half of the N parent ions are involved in each measurement (rather than just one), the Hadamard 2D ICR experiment offers a potential gain of a factor of $\sim N/2$ in speed (for the same S/N) or $\sim (N/2)^{1/2}$ in S/N (for the same total experiment time) over N 1D FT-ICRMS/MS experiments.

The second 2D ICR experiment is

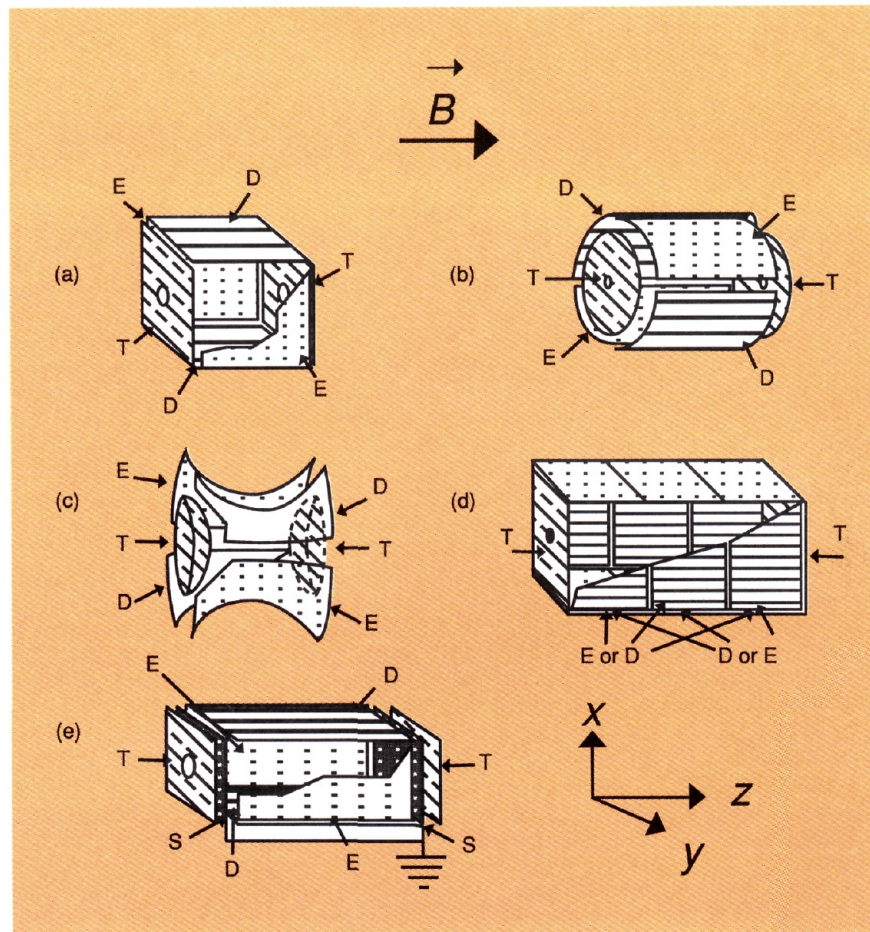


Figure 6. Several ion trap geometries designed for use in FT-ICRMS.

(a) Standard cubic trap. (b) Standard cylindrical trap. (c) Hyperbolic or Penning trap with ring electrode segmented to operate in the standard mode. (d) Elongated and segmented ion trap, designed to facilitate detection in a central electric field-free region. (e) Screened ion trap designed to produce a particle-in-a-box-like potential (see also Figure 10). The excitation, detection, trap, and screen electrodes are designated E, D, T, and S, respectively.

modeled after the so-called NOESY (nuclear Overhauser enhancement spectroscopy) 2D FT-NMR experiment (52). It is based on the principle that ions can be "de-excited" back to their starting points by use of a 180° phase shift in either a single-frequency (53) or frequency sweep (54) excitation. In the 2D FT-ICR experiment, all ions are excited to a given ICR orbital radius; following a variable delay period (whose duration defines the time scale for the second FT), the ions are excited again. Depending on the ICR frequency of the ions of interest, the second excitation will be in phase, out of phase, or somewhere in between with respect to the first. The ICR radius and the translational energy of the parent ion (and hence the abundance of daughter ions) can thus be modulated according to the ICR frequency of the corresponding parent ion by incrementing the delay period in successive experiments (55). In the resulting 2D FT mass spectrum, off-diagonal peaks reveal ion-molecule reactions and/or fragmentation, just as off-diagonal peaks in a NOESY spectrum reveal through-space dipole-dipole coupling between magnetic nuclei.

Electromagnetic pathology: Nonlinear ICR

Readers familiar with FT-NMR spectroscopy will recognize many features it has in common with FT-ICRMS in its linear approximation: SWIFT excitation, 180° pulse, 2D FT spectroscopy, and quadrature excitation and detection (see below). However, the common ground narrows considerably when we consider nonlinear effects, which form the basis for the rest of this article (and much of the recent progress in FT-ICRMS).

Finite electrodes: Trapping and magnetron motions. Typical solenoidal superconducting magnets have good spatial homogeneity (e.g., to within ~ 1 part in 10^5) over the relatively small volume (say, $2.5 \times 2.5 \times 10$ cm) of the ion trap within which an FT-ICR experiment is conducted. As noted earlier, in the absence of an axial (z) component of the electric field, the axial motion of ions is unrestrained. Ions initially formed along the central (z) axis of the solenoid are kept from escaping in the x - y plane by virtue of their ion cyclotron orbital motion. However, to keep ions from escaping along the z -axis, it is necessary to apply a static voltage, V_T (typically a few volts), to each of the two "trapping" electrodes located at $z = \pm c/2$ at each end of the ion trap. Moreover, it is experimentally convenient to excite ICR orbital mo-

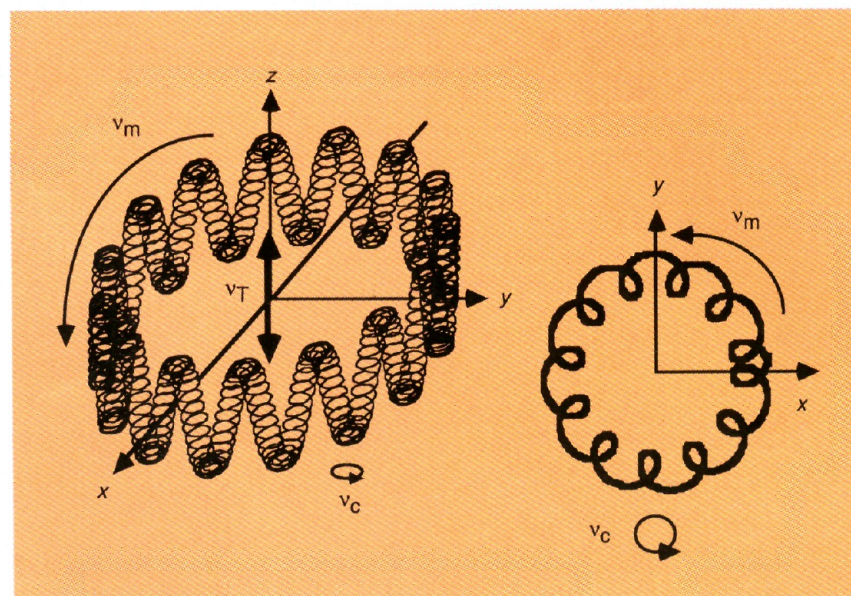


Figure 7. Ionic trajectory (left) within an ion trap, with all three fundamental modes (cyclotron, magnetron, and trapping) excited, and the projection (right) of that trajectory onto the x - y plane.

For clarity, the relative magnitude of the magnetron oscillation has been exaggerated. In typical FT-ICRMS experiments, the magnetron radius is much smaller than the cyclotron radius. (Adapted with permission from Reference 26.)

tion on one opposed pair of electrodes and to detect that motion on a second opposed pair of electrodes. Some of the many ion trap configurations applied to FT-ICRMS over the past few years are shown in Figure 6.

To a good approximation, we may separate the forces and resulting ion motions that are parallel or transverse to the magnetic field (z) axis. Near the center of any of the ion traps of Figure 6, the trapping electric field varies approximately linearly with z (56). Thus ions execute simple harmonic "trapping" oscillation back and forth between the two trapping electrodes, at a trapping frequency

$$\nu_T = (q\alpha V_T / \pi^2 m a^2)^{1/2} \quad (5)$$

in which α is a constant that depends on trap shape (e.g., $\alpha = 1.386$ for a cubic trap).

Just as squeezing a balloon from the ends forces it to bulge out in other directions, "squeezing" ions toward the center of the trap along the z -axis by introduction of a trapping z -potential also produces a force that pushes the ions radially outward from the z -axis. That radially outward force (the x - y component of the first term on the right-hand side of Equation 2) is exactly opposite in direction to the magnetic component of the Lorentz force (second term on the right-hand side of Equation 2). In other words, it is as if the magnetic field strength has been reduced by adding the trapping poten-

tial. Because ICR orbital frequency is proportional to B_0 (Equation 1), we infer that introduction of the trapping potential will lower the observed ICR orbital frequency from its value ($\nu_c = qB_0/2\pi m$) in the absence of the trapping potential.

Fortunately, the electrostatic potential in any of the ion traps in Figure 6 is well approximated (at least, near the center of the trap) by a "quadrupolar" potential (13)

$$V(x,y,z) = V_T [\gamma - (\alpha/a^2)(x^2 + y^2 - 2z^2)] \quad (6)$$

in which α and γ have fixed numerical values for a given trap shape and a is a characteristic trap dimension. Substitution of the resulting electric field, $E = -\nabla V(x,y,z)$, into Equation 2 leads to a system of three linear second-order differential equations. The equation involving only the z -coordinate may be solved independently to yield the sinusoidal trapping motion of Equation 5. The two remaining coupled differential equations in x and y have two solutions (56): the ion cyclotron orbital motion, whose frequency is shifted (downward, as noted above) to

$$\omega_+ = \frac{1}{2} [\omega_c + \omega_c (1 - m/m_{crit})^{1/2}]$$

$$\text{where } m_{crit} = qa^2 B_0^2 / 8\alpha V_T \quad (7a)$$

and a natural magnetron motion at frequency

Table I. Natural ion motional frequencies (Hz) for singly charged ions trapped in a quadrupolar potential (Equation 6) at a static magnetic field strength of 3.0 T^{a,b}

Motion	$m = 100$	1000	10,000	$m_{\text{crit}} = 50,492$
$\nu_+ \approx qB/2\pi m$	460,430	45,837	4,366	456
$\nu_- \approx \alpha V_T/\pi a^2 B$	228	229	240	456
$\nu_T = (\alpha q V_T / \pi^2 m a^2)^{1/2}$	14,496	4,584	1,450	645

Note: Masses are listed in u.

^a Although the cyclotron frequency ν_+ varies strongly with mass, the trapping frequency, ν_T , exhibits a much weaker mass dependence and the magnetron frequency ν_- is nearly mass- and charge-independent.

^b Assumptions: $a = 1.0$ in. (cubic trap); $\alpha = 1.386$ (cubic trap); $B = 3.0$ T; $V_T = 1.0$ V.

$$\omega_- = \frac{1}{2} [\omega_c - \omega_c (1 - m/m_{\text{crit}})^{1/2}] \quad (7b)$$

The three natural ICR motions are illustrated in Figure 7, and typical experimental values are listed in Table 1. We shall next discuss their implications.

ICR orbital frequency shift and mass calibration. From Equation 7a it is clear that the relation between observed ICR orbital frequency, ω_+ , and ionic charge-to-mass ratio, q/m , is no longer linear. As a result, Equation 7a leads to a mass calibration equation that has two adjustable parameters (A and B) rather than one (6):

$$m = A/\nu_+ + B/\nu_+^2 \quad (8)$$

Equation 8 has proved accurate in practice, leading to sub-part-per-million mass measurement accuracy over a wide mass range (e.g., $60 \leq m/z \leq 500$) when an internal calibrator is provided. Addition of more terms to Equation 8 does not materially improve mass measurement accuracy (8).

Reduction of upper mass limit. From Equations 7a and 7b it is clear that above a "critical" mass, m_{crit} , the cyclotron and magnetron frequency expressions become mathematically complex. Physically, what happens is that the outwardly directed electric force can no longer be overcome by the inwardly directed magnetic force: Ions of $m \geq m_{\text{crit}}$ simply spiral radially outward until they strike one of the trap electrodes. In other words, ions of $m > m_{\text{crit}}$ cannot be trapped. The resulting upper mass limit, m_{crit} , can be relatively low (e.g., $\sim 50,000$ u for singly charged ions at 3.0 T in a 1-in. cubic trap with $V_T = 1$ V).

From Equation 7 it is also clear that the upper mass limit may be increased by increasing q (i.e., multiply charged ions), increasing B_0 (larger magnet), in-

creasing a (larger ion trap), reducing V_T (smaller trapping voltage), and/or decreasing α (e.g., changing the trap electrode geometry). Of these options, the simplest and most effective is to change the trap configuration.

Harmonics. Over the past few years, it has become evident that the nonlinearities of the ICR experiment can produce responses not only at the three natural trapping, cyclotron, and magnetron frequencies, but also at various multiple and combination frequencies (see box).

Of these, the easiest to understand is the appearance of spectral signals at (odd) "harmonic" frequencies (57).

Consider an ion executing a perfectly circular orbit centered on the z -axis in a cylindrical ion trap (Figure 8). When the ICR orbital radius, r , is much less than r_0 (the inner radius of the detector electrode), the difference in induced charge between the two opposed detector electrodes is small but nearly sinusoidal. The corresponding FT frequency domain spectrum of that signal therefore consists of a single peak at the "fundamental" or "first harmonic" ICR orbital frequency, ω_+ . However, as the ICR orbital radius approaches r_0 , the detected time domain signal more closely resembles a chopped square wave whose spectrum now contains peaks at both fundamental and odd harmonic frequencies: $M\omega_+$, $M = 1, 3, 5, \dots$ (Only odd harmonics are observed, because the ICR signal is detected "differentially"—as the difference between the signals induced on the two opposed detector electrodes.) In practice, harmonic signals are generally small in magnitude (a few percent) relative to the signal at the fundamental ICR orbital frequency, but they may be exploited or amplified for special applications (see below).

Sidebands. A second type of distortion resulting from nonlinear ICR behavior is modulation, in which a response is observed at combination frequencies between two or all three of the fundamental ICR motions. For example, it is well known that the amplitude of the detected signal from an ion un-

Fundamental frequencies of motion of an ion in an ion trap under the quadrupolar approximation (top) and the frequencies detected with various detection schemes (bottom)

Fundamental ICR frequencies

$$\begin{aligned} \nu_+ &\approx \nu_c - \nu_- \approx \nu_c - \alpha V_T / \pi a^2 B \\ \nu_- &\approx \alpha V_T / \pi a^2 B \\ \nu_T &= (\alpha q V_T / \pi^2 m a^2)^{1/2} \end{aligned}$$

Experimentally observed frequencies

ν_c	(Infinite detection electrodes)
$3\nu_c, 5\nu_c, 7\nu_c, \dots$	(Finite detection electrodes, $V_T = 0$)
$\nu_c, 2\nu_c, 3\nu_c, 4\nu_c, \dots$	(Off-axis ions, finite electrodes, $V_T = 0$)
$\nu_+ \pm \nu_-, \nu_+ \pm 2\nu_-, \dots$	(Single detection electrode: $\nu_+ + \nu_- = \nu_c$)
$\nu_+ \pm 2\nu_-, \nu_+ \pm 4\nu_-, \dots$	(Differential two-electrode detection)
$\nu_+ \pm \nu_T, \nu_+ \pm 2\nu_T, \dots$	(Trap and magnetic field axes not parallel)
$\nu_+ \pm 2\nu_T, \nu_+ \pm 4\nu_T, \dots$	(Trap and magnetic field axes parallel)
$\nu_T, 3\nu_T, 5\nu_T, \dots$	(Differential detection on trapping plates)
$2\nu_T, 4\nu_T, \dots$	(Differential two-electrode detection)
$\nu_c, 2\nu_+, 2\nu_-$	(Quadrupole detection mode)

^a Some observable frequencies are not mentioned because they are of no interest. In general, the higher the order of the harmonic or sideband, the lower its relative magnitude.

dergoing cyclotron motion depends on the axial position of the ion (9, 11, 12). In particular, the amplitude of the signal at frequency, ω_+ , is maximal at the center of the trap ($z = 0$) and minimal at the trap plates where it actually drops to zero. Thus, for an ion undergoing combined cyclotron and trapping motions, the FT spectrum of the observed time domain ICR signal exhibits sidebands at $\omega_+ \pm 2\omega_T$, which have been observed experimentally (16). From symmetry arguments, it is possible to show that there should be no sidebands at $\omega_+ \pm \omega_T$ in a properly aligned trap; the magnitude of any such sidebands therefore provides a useful diagnostic index for aligning the trap with respect to the applied magnetic field. Magnetron sidebands (e.g., $\omega_+ \pm n\omega_-$, $n = 1, 2, \dots$) have also been observed; their utility will be discussed later.

The z-excitation: Mass-dependent mass spectral peak magnitudes. Up to now, we have considered the effects of the true static electric field. However, the rf electric field is nonuniform because of the finite dimensions of the transmitter electrodes and the presence of the remaining detector and trap electrodes, which warp

the rf electric field between the transmitter electrodes. There are at least three direct consequences of nonuniform rf electric field.

First, the effective rf electric excitation field is weaker than that predicted from the infinite electrode approximation (e.g., by a factor of ~ 0.72 for a cubic trap [10, 15]).

Second, because the electric field lines curve rather than extend in straight lines between the two transmitter electrodes, an rf electric field excitation in the x -direction will have a component along the z direction. If that component happens to oscillate at twice the trapping frequency (or even at one of the cyclotron/trapping sidebands), ions will be excited (or even ejected) axially as the result of transverse excitation (15, 17–19). The effect is mass dependent: For a given irradiation period at twice the trapping frequency, lowest mass ions gain the most energy and are more readily ejected. Because the rf electric field curvature varies with radial distance from the z -axis, the ejection effect varies with ICR orbital radius, leading to mass- and radius-dependent FT-ICR relative mass spectral peak heights (17).

Third, the transverse component of

the rf electric field is strongest near the midplane ($z = 0$) of the trap and weakens as one proceeds toward either trap electrode. Thus ions with low trapping amplitude will be excited to higher ICR orbital radius than ions of large trapping amplitude. Also, because ICR orbital frequency varies with ICR orbital radius in a nonquadrupolar trap, the effect is to produce inhomogeneous line-broadening caused by a superposition of signals of different ICR orbital frequency from ions of different trapping oscillation amplitude and/or different ICR orbital radius (14).

Description, exploitation, and/or elimination of nonlinear effects

The problems resulting from nonlinear ICR behavior are empirically well known but have only recently been quantitatively analyzed or rectified. In this section, we try to show how a better description of the problems has led to some remarkable improvements in the performance and reliability of the FT-ICR technique.

In search of a quadrupolar potential: Hyperbolic trap. A perfect quadrupolar electrostatic potential (Equation 6) offers the very important advantage that the ICR orbital frequency, ω_+ of Equation 7a, is independent of ICR orbital radius (6, 56). Thus there is no “spread” in ICR frequencies (inhomogeneous spectral peak broadening) for ions with different ICR motional amplitude. Most early ICR ion trap configurations produce an approximately quadrupolar field only near the trap center. Fortunately, there is a trap geometry that produces a near-perfect quadrupolar potential: a “hyperbolic” trap (see Figure 6c) formed from a “ring” electrode and two “end caps,” all of whose surfaces are hyperboloids of revolution (56).

If the “ring” electrode is unbroken, it turns out that ions must be introduced off axis to provide for “parametric” excitation and detection (6). Alternatively, the “ring” electrode may be cut along two perpendicular planes to yield a trap that is configured just like a cubic trap except that the electrode surfaces are curved (58). We have shown that such a segmented hyperbolic trap indeed reduces FT-ICR spectral peak widths and also improves mass accuracy based on the quadrupolar mass calibration formula of Equation 8. However, the hyperbolic trap has the following disadvantages: The curved electrodes produce a highly nonuniform rf excitation field, further exacerbating problems associated with z -ejection (see above); and the static electric field quadrupolar potential produces a radial electric field, $E(r) = E_0r$, which re-

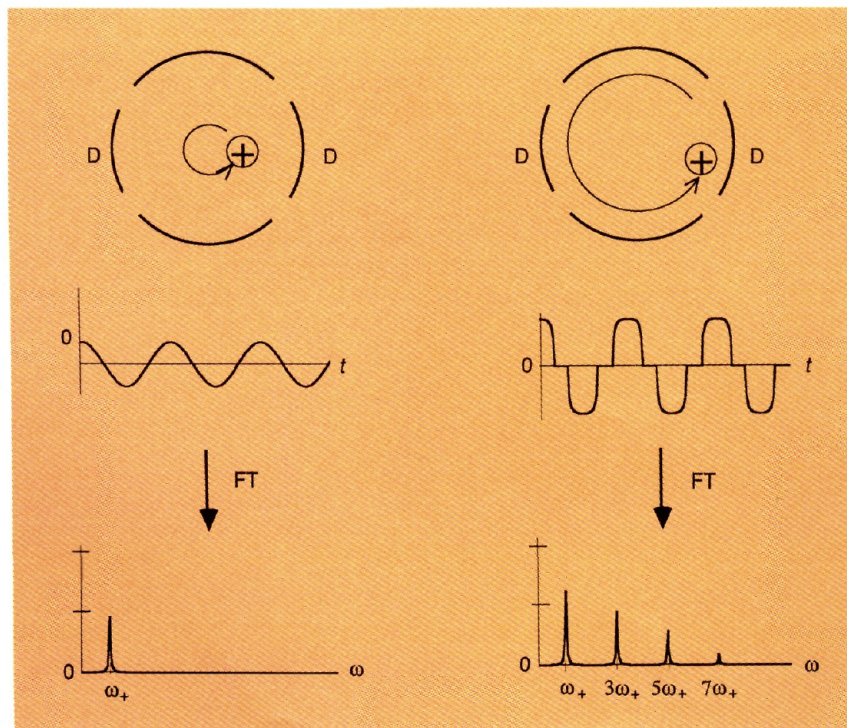


Figure 8. Origin of odd-integer harmonic signals in FT-ICR mass spectra, illustrated for a positive ion moving in a circular orbit in a cylindrical ion trap.

Left: The time domain ICR signal induced on opposed cylindrical detector electrodes, D, is small but approximately sinusoidal when the ICR orbital radius, r , is much smaller than the radius, r_0 , of the detector electrode. The corresponding FT frequency spectrum therefore consists of a single peak at the fundamental ICR orbital frequency, ω_+ . Right: As r approaches r_0 , the detected time domain signal approaches a square wave whose spectrum contains peaks at all odd harmonics of the fundamental ICR frequency of the ion. (Adapted with permission from Reference 26.)

duces the upper mass limit (see above) as in the tetragonal and cylindrical traps.

Quantitating ion behavior for nonhyperbolic traps: Reciprocity. Because even a perfectly quadrupolar trap is not optimally suited for FT-ICRMS, we are forced to consider other trap geometries. Unfortunately, the algebraic complexity of computing the electric field (rf plus static) and the ICR signal (from the differential charge induced between two opposed detector electrodes) can become truly formidable. For example, the electrostatic potential alone for a simple tetragonal trap of length, c , and cross-sectional width, a , is given by

$$V(x, y, z) = \frac{16V_T}{\pi^2} \times \sum_{m,n=0}^{\infty} \left\{ (-1)^{m+n} \cos \left[\frac{(2m+1)\pi x}{a} \right] \times \cos \left[\frac{(2n+1)\pi y}{a} \right] \cosh \left[\frac{k_{mn}\pi z}{a} \right] / (2m+1)(2n+1) \cosh \left[\frac{k_{mn}\pi c}{2a} \right] \right\} \quad (9)$$

in which $k_{mn} \equiv [(2m+1)^2 + (2n+1)^2]^{1/2}$ and the geometric center of the trap is taken as the coordinate frame origin (56). Moreover, it is much more difficult to compute the induced ICR signal than to compute the electric potential for the same arrangement.

Fortunately, the simple relation between the excitation and detection "fields," shown (for infinitely extended electrodes) in Figure 2, turns out to be a special case of the very useful "reciprocity" theorem (12). One way of stating the theorem is that the potential (in volts) at a given point in the trap, produced by applying $+1$ V and -1 V to two opposed "transmitter" electrodes, is numerically identical to the differential charge that would be induced between the same two (grounded) electrodes by placing a unit charge at that same point. In other words, if (as is generally the case) we are able to obtain an algebraic expression for the potential at any point within a particular ion trap with ± 1 V applied to the two detection electrodes ($+1$ V to one, -1 V to the other), then we have automatically solved the converse problem of determining the ICR signal for an ion at the same point—we need simply compute the ICR signal for each of 100 points around the circumference of one ICR orbit (in steps of 3.6° each) and Fourier transform it to discover the FT-ICR frequency spectrum for ions following that trajectory.

ICR orbital radius and ion energy determination. Nonlinear effects are not all bad. For example, such useful devices as laser-doubling crystals and rf mixers are based on nonlinear phenomena (26). We may therefore seek to capitalize on some of the nonlinear effects of ICR. For example, the relative magnitudes of the first, third, fifth, ... harmonics increase with ICR orbital radius, r , approximately as r, r^3, r^5, \dots (59). Thus the experimentally measurable ratio of the magnitude of the third harmonic to that of the first harmonic, $M(3\omega_+)/M(\omega_+)$, increases approximately as the square of the ICR orbital radius (Figure 9). Thus measurement of $M(3\omega_+)/M(\omega_+)$ provides the first direct measure of the orbital cyclotron radius of an excited ion (and thus its translational energy).

Moreover, now that we are able to calculate the ICR signal induced by an ion at a given ICR orbital radius, we should be able to determine the number of ions from their measured radius and measured ICR signal. These new tools should prove exceedingly valuable for testing current theories of ICR signal relaxation: for example, loss of ions from a coherently orbiting packet, diffusion of a packet of ions around their cyclotron orbit, decrease in ICR orbital radius, and ion-molecule momentum transfer collision mechanism.

As an alternative to measuring cyclotron radii, we have expressed the exact excitation potential in cylindrical coordinates to compute the postexcitation cyclotron radius of ions in response to on-resonance single-frequency excitation. We find that the infinite electrode model overestimates the ICR orbital radius by a factor of ~ 1.39 for a cubic trap. Because the translational energy, $q^2B_0^2r^2/2m$, of an rf-excited ion varies as the square of its ICR orbital radius, we find that ions in a cubic trap are excited to only about half the energy previously estimated from the infinite electrode model (which had been used to determine collisionally induced dissociation energy thresholds).

We have been able to demonstrate good agreement between the experimental and calculated onset of radial ejection attributable to rf electric field excitation in a cubic trap (10). Our results allow for similar computations for tetragonal or cylindrical traps of arbitrary aspect (i.e., length-to-width) ratio (10, 11). Fortunately, the rate of increase of ICR orbital radius with the product of rf electric field excitation magnitude and duration is still approximately linear, but with a slope reduced by a factor of ~ 0.72 , and thus does not pose a problem for most routine analytical work.

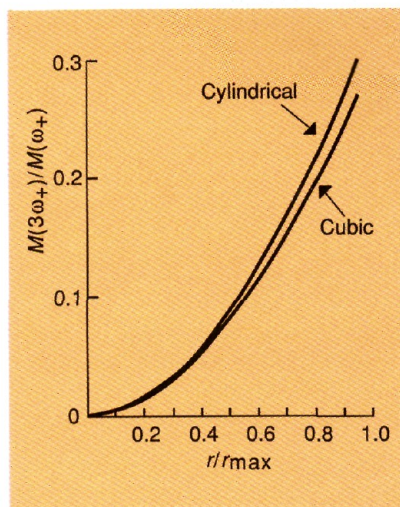


Figure 9. Ratio of the magnitude of the third harmonic to that of the fundamental, $M(3\omega_+)/M(\omega_+)$, versus ICR orbital radius, r , for cylindrical ($c/2r_{\max} = 1$) and cubic ion traps.

Both curves are approximately quadratic. From such curves, the ICR orbital radius (and thus ion orbital translational energy) may be determined directly from experimental FT-ICRMS magnitude mode peak heights. (Adapted from Reference 60.)

Shimming the static electric field:

Screened trap. The two general ways to approach physical problems are to seek a complete mathematical description of the conventional system or to devise a new system for which the desired behavior is realized more closely. FT-ICRMS ion traps offer good examples of each approach.

Until recently, it was thought that the optimal trap geometry for FT-ICR should be hyperbolic; that is, $V(x, y, z) - V(0, 0, 0) = (\alpha V_T/a^2)[2z^2 - (x^2 + y^2)]$, so as to produce simple harmonic oscillation in ion position along the z -axis and a position-independent cyclotron frequency. However, as noted above, the trapping potential that is applied axially is necessarily accompanied by a radially outward electric field that shifts the ICR orbital frequency in a mass-dependent way and reduces the upper mass limit. Furthermore, the excitation field in such a trap has a strong axial component that may exacerbate z -ejection problems.

In 1989 we introduced a new kind of ion trap in which grounded screens are placed just inside the trapping electrodes (60). Just as a bubble can penetrate through a screen door by only about one mesh spacing, the electric field from the trapping plates is effectively shielded from ions in the trap until the ions nearly touch the screens. In other words, we have effectively replaced the harmonic oscillator potential by the simpler particle-in-a-box

potential, as shown in Figure 10. The electrostatic potential in the trap is reduced by a factor of up to 100, virtually eliminating ICR orbital frequency shifts (and thereby improving mass resolution, mass accuracy, and selectivity for ion excitation or ejection) by eliminating the unwanted radial electric field. The screened trap should significantly extend the FT-ICR upper mass limit for the same reasons. The effect of the screened trap is similar to that of an elongated trap (61, 62); the advantage of the screened trap is that the near-zero electric field region is produced in a smaller volume over which the magnetic field is more uniform.

Shimming the rf electric field: **Guard wires.** From the previous section, the reader may have guessed that it is also possible to design an ion trap for which the rf excitation electric field is more uniform than that of a conventional tetragonal, cylindrical, or hyperbolic trap. The trick here is to shim ("unwarp") the rf electric field by adding conductive elements whose positions and rf voltages are adjusted so as to flatten the rf field and make it spatially uniform anywhere between the two transmitter electrodes. The problems associated with the nonuniform excitation field were discussed earlier.

Figure 11 shows one of several possible rf-shimmed ion trap designs (63, 64) and the resultant improvement in rf electric field homogeneity. With our rf-shimmed trap, the variation in relative FT-ICR mass spectral peak heights with ICR orbital radius was reduced from a factor of more than 10 down to a few percent for a cubic trap. Even better quantitative precision should be possible with somewhat elongated ion traps that reduce the effects of electrostatic field nonuniformity. Finally, we note that the rf-shimmed trap of Figure 11 effectively incorporates some of the advantages of the screened trap with those of the rf-shimmed trap by its placement of shim wires in front of the trapping electrodes.

Quadrature excitation and detection. Until recently, FT-ICRMS was conducted with linearly polarized rf excitation and detection (i.e., use of just one pair of opposed electrodes for excitation and a second pair for detection). It can be shown that this configuration is half as efficient as quadrature excitation and detection, in which both pairs of electrodes are active simultaneously.

The inefficiency of the standard mode of operation during the excitation event can be understood as follows: The orbits of positive ions all rotate in the same sense (counterclockwise, when viewed along a magnetic

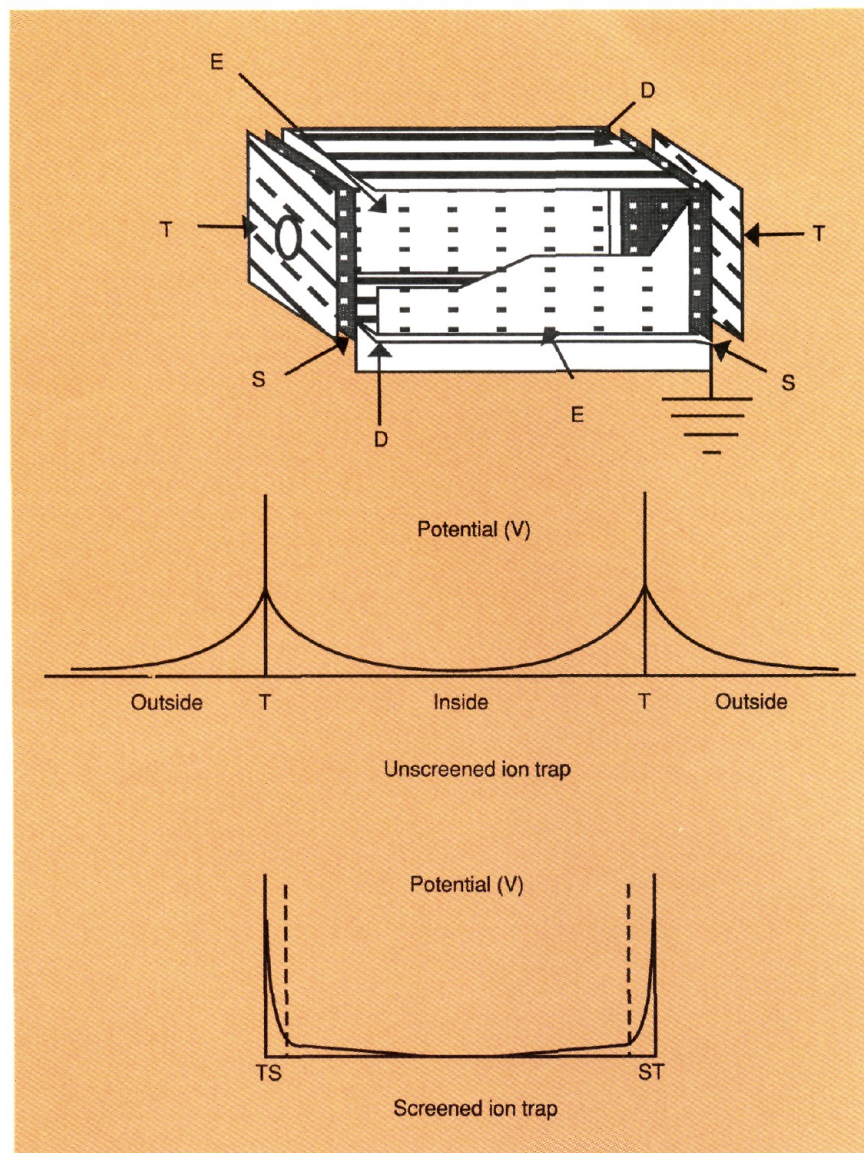


Figure 10. Screened tetragonal ion trap.

A conductive screen, typically 10–20 wires per inch, is placed in front of each trapping electrode. Holding the screens at ground potential produces the particle-in-a-box potential along the z-axis of the trap shown at the bottom of the figure. For comparison, the axial potential for the corresponding unscreened trap is also shown (middle). Note that the screens effectively shield most of the trap volume from the (mostly undesirable) effects of the trapping potential (see text). The excitation, detection, trap, and screen electrodes are designated E, D, T, and S, respectively.

field directed into the plane of the paper). The linearly polarized excitation field may be decomposed into two counter-rotating (clockwise and counterclockwise) electric fields, of which the clockwise-rotating component has almost no net effect upon the ions. Thus half of the excitation field magnitude is wasted.

By introducing a second pair of opposed excitation plates with an excitation waveform that is phase-shifted 90° relative to the first pair, we can construct a circularly polarized excitation field that rotates in the same sense as the ions. The resulting quadrature excitation is clearly twice as efficient as

its linearly polarized counterpart.

The argument that demonstrates the relative efficiency of quadrature detection proceeds similarly: By using only one pair of detection plates, we obtain a linearly polarized time domain signal. In other words, the detector cannot distinguish between clockwise and counterclockwise rotation, even though the ions are actually rotating in only one sense.

By detecting simultaneously and independently from a second pair of opposed plates oriented at 90° relative to the first pair, we can distinguish between clockwise and counterclockwise components: The time domain signals

from the two pairs of plates are identified as real and imaginary components of a mathematically complex input to the FFT algorithm, and the clockwise and counterclockwise components are then manifested as negative- and positive-frequency peaks in the resulting FT spectrum. Thus, for a given coherently rotating ion packet, quadrature detection yields a S/N that is higher by a factor of $\sqrt{2}$ (i.e., signal increased by a factor of 2 and noise increased by a factor of $\sqrt{2}$) than would be obtained with linearly polarized detection.

Several groups have recently demonstrated various forms of quadrature detection, based either on independent acquisition of signals from two pairs of opposed detector electrodes (65) or (for heterodyne mode only) on splitting the signal from one pair of detector electrodes in half and phase-shifting one of the two signals by 90° (66, 67). The FT data reduction is essentially the same, except that the raw data from linearly polarized detection are treated as mathematically real, whereas each pair of data points from the two quadrature channels is treated as mathematically complex (one real, the other imaginary). Various nuances of quadrature data reduction and display are discussed at length elsewhere (26).

Multipole excitation and detection. Quadrature excitation and detection offer one of many recently explored multiple-electrode arrangements for FT-ICRMS. Perhaps the most clever and useful is the quadrupole detection scheme of Schweikhard et al. (68). The signals from one pair of opposed detector electrodes are added together and then subtracted from the sum of the signals from the second pair of opposed detector electrodes oriented perpendicular to the first pair. Depending on the relative magnitudes of the cyclotron and magnetron orbital radii (which can be varied in their experiment), the FT-ICR frequency (mass) spectrum contains a harmonic signal at $2\nu_+$ and (more interestingly) a new signal at the sum of the cyclotron and magnetron frequencies ($\nu_+ + \nu_-$).

The striking advantage of this experiment is now evident from Equation 7: namely, $(\nu_+ + \nu_-) = \nu_c$. In other words, this experiment extracts the unshifted ion cyclotron orbital frequency, even though ions are trapped by the usual quadrupolar potential, which would shift the conventionally detected signal, ν_+ , to a value lower than ν_c . This same sideband can be generated from more conventional traps by grounding either of the detection electrodes and ensuring that both modes are excited as shown by Allemann et al. (69). Magnetron motion has also been

observed directly (70).

Several research groups have devised ion traps specifically designed to increase the strength of various harmonic signals at the expense of the fundamental (57, 71, 72). Such designs were motivated by the hope that mass resolving power might increase with harmonic order, because two closely spaced peaks are three times farther apart at the third harmonic than at their fundamental ICR orbital frequencies. However, the precision with which an ICR signal (or any other discretely sampled spectral signal) can be determined is proportional to the product of S/N and the square root of the number of data points per linewidth (73).

Because the maximum magnitude of

the M th harmonic signal is in general less than $1/M$ of that of the fundamental signal for conventional two-electrode differential detection in standard traps (10), detection of the M th harmonic signal thus offers no theoretical advantage in precision (e.g., for accurate mass determination) over detection at the fundamental ICR orbital frequency. In other words, for conventional ICR detection, the harmonic peaks may be farther apart, but their smaller magnitudes more than make up for their increased peak separation, with respect to mass measurement accuracy.

Various multielectrode ion trap designs can increase the strength of harmonic signals at the expense of the fun-

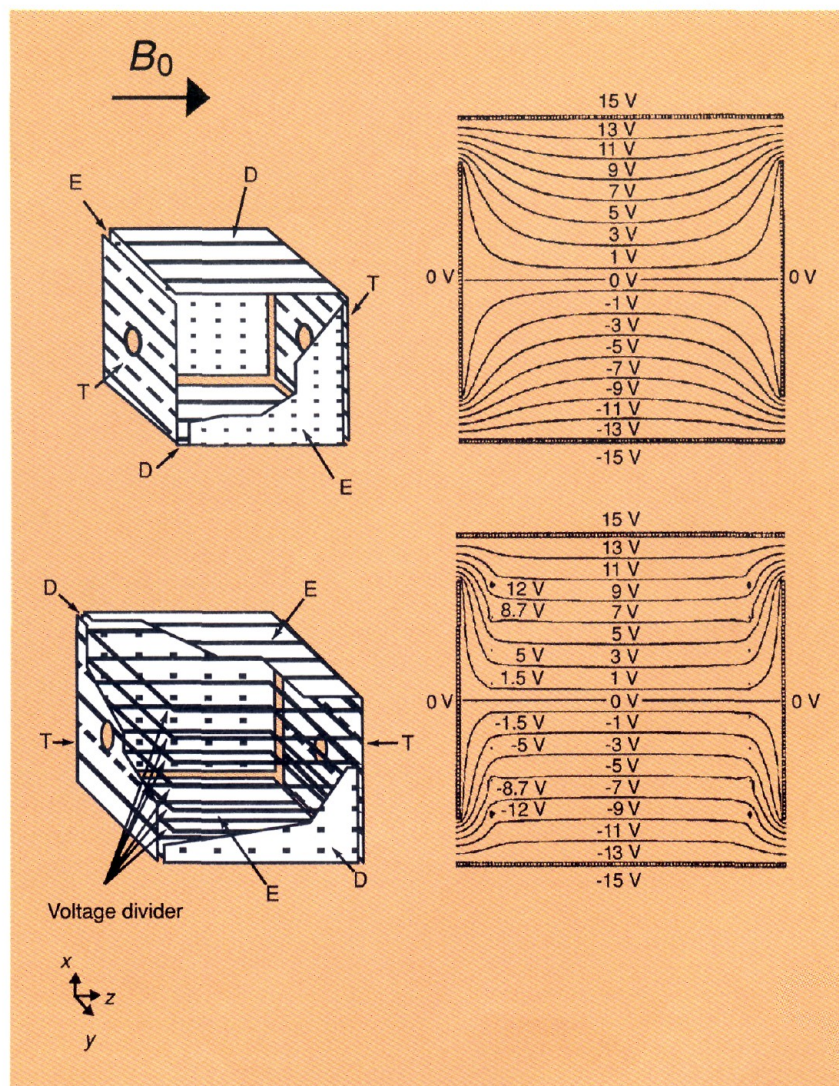


Figure 11. Standard (top left) and rf-shimmed (bottom left) cubic ion traps and their corresponding rf isopotential contours (right).

An rf potential of ± 15 V is applied to the excitation electrodes, with rf potentials of decreasing magnitude applied to the shim wires as shown. Note the much flatter rf isopotential contours (and thus much more uniform rf electric field magnitude) for the rf-shimmed trap, with resultant elimination of mass-dependent z-ejection (see text). The excitation, detection, and trap electrodes are designated E, D, and T, respectively.

damental to overcome the factor of $1/M$ loss in S/N that is inherent in conventional two-electrode detection. Unfortunately, a detailed analysis shows that the spectral linewidth is not necessarily independent of M (59); furthermore, one always encounters multiple peaks corresponding to the same m/q , leading to more complex mass spectra.

Directions for future research

We have considered recent developments in our fundamental understanding of the processes of ion trapping, excitation, and detection in FT-ICRMS. An additional ongoing major development not treated here is the external injection of ions through the fringing field of a solenoidal superconducting magnet. Such injection has made possible the coupling of various ion sources (e.g., laser desorption [36], fast atom bombardment [74], supersonic jet [75], Cs⁺ ion beam [76], SF₆ neutral beam [77], field desorption [78], ²⁵²Cf plasma desorption [79], electrospray [80], and high-pressure ionization [81]) to an FT-ICR mass spectrometer for ultrahigh resolution mass analysis. In addition, many papers describing improvements in acquisition and reduction of the inherently discrete data sets involved in FT-ICRMS have appeared. For these and other aspects, the reader is referred to any of several recent reviews (32–49).

The FT-ICRMS technique has matured significantly over the past five years. The SWIFT technique makes it possible to produce optimally uniform and optimally selective excitation and ejection for ion selection and detection. Analytic algebraic expressions for the electric potential (static plus rf) and for the detected ICR signal in tetragonal and cylindrical ion traps of arbitrary length-to-width ratio are now available. Those expressions can be exploited to determine directly ICR orbital radius and energy as well as the number of excited ions in the trap. Moreover, we now understand the origin (and can control the relative magnitudes of) signals at various harmonic and combination frequencies.

Finally, we are now able to devise nonquadrupolar ion traps with highly uniform static and rf electric fields, thereby reducing or eliminating prior limitations on mass accuracy, upper mass limit, selectivity of ion excitation or ejection, and relative ion abundance precision and reproducibility. The way is now cleared for applications of FT-ICRMS to the full range of mass spectrometric analysis.

Because most of the existing FT-ICR mass spectrometers were acquired before the advent of the above-men-

tioned improvements, it is reasonable to project that the next doubling period for growth in the number of FT-ICR instruments should be much shorter than the first.

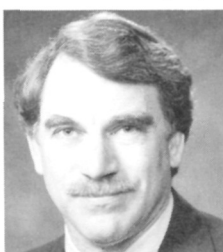
This work was supported by National Science Foundation grant no. CHE-8721498 and The Ohio State University.

References

- (1) Wineland, D. J. *Science* **1984**, *226*, 395–400.
- (2) Comisarow, M. B.; Marshall, A. G. *Chem. Phys. Lett.* **1974**, *25*, 282–83.
- (3) a. Comisarow, M. B. *Int. J. Mass Spectrom. Ion Proc.* **1978**, *26*, 369–78; b. Comisarow, M. B. *J. Chem. Phys.* **1978**, *69*, 4097.
- (4) Ledford, E. B., Jr.; Ghaderi, S.; White, R. L.; Spencer, R. B.; Kulkarni, P. S.; Wilkins, C. L.; Gross, M. L. *Anal. Chem.* **1980**, *52*, 463–68.
- (5) Franc, T.; Sherman, M. G.; Hunter, R. L.; Locke, M. J.; Bowers, W. D.; McIver, R. T., Jr. *Int. J. Mass Spectrom. Ion Proc.* **1983**, *54*, 189–99.
- (6) Ledford, E. B., Jr.; Rempel, D. L.; Gross, M. L. *Anal. Chem.* **1984**, *56*, 2744–48.
- (7) Rempel, D. L.; Ledford, E. B., Jr.; Huang, S. K.; Gross, M. L. *Anal. Chem.* **1987**, *59*, 2527–32.
- (8) Wang, M.; Marshall, A. G. *Int. J. Mass Spectrom. Ion Proc.* **1989**, *86*, 31–51.
- (9) Rempel, D. L.; Huang, S. K.; Gross, M. L. *Int. J. Mass Spectrom. Ion Proc.* **1986**, *70*, 163–84.
- (10) Grosshans, P. B.; Marshall, A. G. *Int. J. Mass Spectrom. Ion Proc.* **1990**, *100*, 347–79.
- (11) Grosshans, P. B.; Marshall, A. G., The Ohio State University, unpublished results.
- (12) Dunbar, R. C. *Int. J. Mass Spectrom. Ion Proc.* **1984**, *56*, 1–9.
- (13) Jeffries, J. B.; Barlow, S. E.; Dunn, G. H. *Int. J. Mass Spectrom. Ion Proc.* **1983**, *54*, 169–87.
- (14) Rempel, D. L.; Gross, M. L. Presented at the 2nd American Society for Mass Spectrometry Sanibel Conference on Ion Trapping in Mass Spectrometry, Sanibel Island, FL, January 1990.
- (15) van der Hart, W. J.; van de Guchte, W. J. *Int. J. Mass Spectrom. Ion Proc.* **1988**, *82*, 17–31.
- (16) DeLong, S. E.; Mitchell, D. W.; Cherniak, D. J.; Harrison, T. M. *Int. J. Mass Spectrom. Ion Proc.* **1989**, *91*, 273–82.
- (17) Kofel, P.; Alleman, M.; Kellerhals, H.; Wanczek, K.-P. *Int. J. Mass Spectrom. Ion Proc.* **1986**, *74*, 1–12.
- (18) Alleman, M.; Kofel, P.; Kellerhals, H.; Wanczek, K.-P. *Int. J. Mass Spectrom. Ion Proc.* **1987**, *75*, 47–54.
- (19) Huang, S. K.; Rempel, D. L.; Gross, M. L. *Int. J. Mass Spectrom. Ion Proc.* **1986**, *72*, 15–31.
- (20) Dehmelt, H.; Wineland, D. J. *Bull. Am. Phys. Soc.* **1973**, *18*, 1571.
- (21) Comisarow, M. B.; Marshall, A. G. *J. Chem. Phys.* **1976**, *64*, 110–19.
- (22) Alleman, M.; Kellerhals, H.; Wanczek, K.-P. *Int. J. Mass Spectrom. Ion Proc.* **1983**, *46*, 139–42.
- (23) Bamberg, M.; Alleman, M.; Wanczek, K.-P. *Proceedings of the 35th American Society for Mass Spectrometry Conference on Mass Spectrometry & Allied Topics*; Denver, CO, May 1987; pp. 1116–17.
- (24) Wang, M.; Marshall, A. G. *Int. J. Mass Spectrom. Ion Proc.* **1990**, *100*, 323–46.
- (25) Jackson, J. D. *Classical Electroynamics*; John Wiley and Sons, Inc.: New York, 1975.
- (26) Marshall, A. G.; Verdin, F. R. *Fourier Transforms in Optical, NMR, and Mass Spectrometry: A User's Handbook*; Elsevier: Amsterdam, 1990.
- (27) McIver, R. T., Jr.; Hunter, R. L.; Baykut, G. *Anal. Chem.* **1989**, *61*, 489–91.
- (28) McIver, R. T., Jr.; Baykut, G.; Hunter, R. L. *Int. J. Mass Spectrom. Ion Proc.* **1989**, *89*, 343–58.
- (29) Comisarow, M. B.; Marshall, A. G. *Chem. Phys. Lett.* **1974**, *26*, 489–90.
- (30) Marshall, A. G.; Roe, D. C. *J. Chem. Phys.* **1980**, *73*, 1581–90.
- (31) Marshall, A. G.; Wang, T.-C.L.; Ricca, T. L. *J. Am. Chem. Soc.* **1985**, *107*, 7893–97.
- (32) Marshall, A. G.; Wang, T.-C.L.; Chen, L.; Ricca, T. L. In *Fourier Transform Mass Spectrometry: Evolution, Innovation, and Applications*; Buchanan, M.V., Ed.; ACS: Washington, DC, 1987; pp. 21–33.
- (33) Asamoto, B. *Spectroscopy* **1988**, *3*, 38–46.
- (34) Buchanan, M. V.; Comisarow, M. B. In *Fourier Transform Mass Spectrometry: Evolution, Innovation, and Applications*; Buchanan, M.V., Ed.; ACS: Washington, DC, 1987; pp. 1–20.
- (35) Chiarelli, M. P.; Gross, M. L. In *Analytical Applications of Spectroscopy*; Creaser, C. S.; Davies, A.M.C., Eds.; Royal Society of Chemistry: London, 1988; pp. 263–73.
- (36) *Lasers in Mass Spectrometry*; Lubman, D. M., Ed.; Oxford University Press: New York, 1990; Chapter 7, pp. 11–15.
- (37) Cody, R. B. *Analysis* **1988**, *16*, 30–36.
- (38) Freiser, B. S. In *Techniques for the Study of Ion Molecule Reactions*; Farrar, J. M.; Saunders, W. H., Jr., Eds.; Wiley: New York, 1988; Chapter 2, pp. 61–118.
- (39) Freiser, B. S. *Chemtracts—Anal. Phys. Chem.* **1989**, *1*, 65–109.
- (40) Gord, J. R.; Freiser, B. S. *Anal. Chim. Acta* **1989**, *225*, 11–24.
- (41) Hanson, C. D.; Kerley, E. L.; Russell, D. H. In *Treatise on Analytical Chemistry*, 2nd ed.; Winefordner, J. D., Ed.; Wiley: New York, 1988; Vol. 11, Chapter 2; pp. 117–87.
- (42) Marshall, A. G. *Acc. Chem. Res.* **1985**, *18*, 316–22.
- (43) Marshall, A. G. *Adv. Mass Spectrom.* **1989**, *11A*, 651–69.
- (44) Nibbering, N.M.M. *Adv. Phys. Org. Chem.* **1988**, *24*, 1–55.
- (45) Nibbering, N.M.M. *Acc. Chem. Res.* **1990**, *23*, 279–85.
- (46) Russell, D. H. *Mass Spectrom. Rev.* **1986**, *5*, 167–89.
- (47) Sharpe, P.; Richardson, D. E. *Coord. Chem. Rev.* **1989**, *93*, 59–85.
- (48) Wanczek, K.-P. *Int. J. Mass Spectrom. Ion Proc.* **1989**, *95*, 1–38.
- (49) Wilkins, C. L.; Chowdhury, A. K.; Nuwaysir, L. M.; Coates, M. L. *Mass Spectrom. Rev.* **1989**, *8*, 67–92.
- (50) Mullen, S. L.; Marshall, A. G. *J. Am. Chem. Soc.* **1988**, *110*, 1766–74.
- (51) Williams, E. R.; Loh, S. Y.; McLafferty, F. W.; Cody, R. B. *Anal. Chem.* **1990**, *62*, 698–703.
- (52) Ernst, R. R.; Bodenhausen, G.; Woyna, A. *Principles of Nuclear Magnetic Resonance in One and Two Dimensions*; Clarendon: Oxford, 1987.
- (53) Marshall, A. G.; Wang, T.-C.L.; Ricca, T. L. *Chem. Phys. Lett.* **1984**, *105*, 233–36.
- (54) Noest, A. J.; Kort, C.W.F. *Comput. Chem.* **1983**, *7*(2), 81–86.

- (55) Pfändler, P.; Bodenhausen, G.; Rapin, J.; Walser, M.-E.; Gäumann, T. *J. Am. Chem. Soc.* 1988, 110, 5625-28.
- (56) a. Byrne, J.; Farago, P. S. *Proc. Phys. Soc. London* 1965, 86, 801-20; b. See also Sharp, T. E.; Eyler, J. R.; Li, E. *Int. J. Mass Spectrom. Ion Phys.* 1972, 9, 421-39.
- (57) Pan, Y. P.; Ridge, D. P.; Rockwood, A. L. *Int. J. Mass Spectrom. Ion Proc.* 1988, 84, 293-304.
- (58) Wang, M.; Ledford, E. B., Jr.; Marshall, A. G. *Abstracts of Papers, FACSS XIV*, Detroit, MI; FACSS: October 1987; Abstract 43.
- (59) a. Grosshans, P. B.; Shields, P.; Marshall, A. G. *J. Am. Chem. Soc.* 1990, 112, 1275-77; b. Nikolaev, E. N.; Gorshkov, M. V. *Int. J. Mass Spectrom. Ion Proc.* 1985, 64, 115-25.
- (60) Wang, M.; Marshall, A. G. *Anal. Chem.* 1989, 61, 1288-93.
- (61) Hunter, R. L.; Sherman, M. G.; McIver, R. T., Jr. *Int. J. Mass Spectrom. Ion Phys.* 1983, 50, 259-74.
- (62) Marshall, A. G.; Grosshans, P. B.; Wang, M.; Ricca, T. L.; Ledford, E. B., Jr. *Proceedings of the 36th American Society for Mass Spectrometry Conference on Mass Spectrometry and Allied Topics*; San Francisco, CA, June 1988; pp. 592-93.
- (63) Wang, M.; Marshall, A. G. *Anal. Chem.* 1990, 62, 515-20.
- (64) Hanson, C. D.; Castro, M. E.; Kerley, E. L.; Russell, D. H. *Anal. Chem.* 1990, 62, 520-26.
- (65) Verdun, F. R.; Mullen, S. L.; Ricca, T. L.; Marshall, A. G. *Adv. Mass Spectrom.* 1988, 11A, 670-71.
- (66) Wachter, E. A.; Farrar, T. C.; Kontney, M. J. *Int. J. Mass Spectrom. Ion Proc.*, in press.
- (67) Fujiwara, M.; Kataura, H.; Inoue, M. *Rapid Commun. Mass Spectrom.* 1990, 4, 237-38.
- (68) Schweikhart, L.; Lindinger, M.; Kluge, H.-J. *Int. J. Mass Spectrom. Ion Proc.* 1990, 98, 25-33.
- (69) Allemann, M.; Kellerhals, H.; Wanzenk, K.-P. *Chem. Phys. Lett.* 1981, 84, 547-51.
- (70) Dunbar, R. C.; Chen, J. H.; Hayes, J. D. *Int. J. Mass Spectrom. Ion Proc.* 1984, 57, 39-56.
- (71) Pan, Y. P.; Ridge, D. P.; Wronka, J.; Rockwood, A. L. *Rapid Commun. Mass Spectrom.* 1987, 1(7/8), 120-21.
- (72) Nikolaev, E. N.; Gorshkov, M. V.; Mordehai, A. V.; Talrose, V. L. *Rapid Commun. Mass Spectrom.* 1990, 4, 144-46.
- (73) Chen, L.; Cottrell, C. E.; Marshall, A. G. *Chemom. Intell. Lab. Syst.* 1986, 1, 51-58.
- (74) Hunt, D. F.; Shabanowitz, J.; McIver, R. T., Jr.; Hunter, R. L.; Syka, J. E. P. *Anal. Chem.* 1985, 57, 765-68.
- (75) Alford, J. M.; Williams, P. E.; Trevor, D. J.; Smalley, R. E. *Int. J. Mass Spectrom. Ion Proc.* 1986, 72, 33-51.
- (76) Hunt, D. F.; Shabanowitz, J.; Yates, J. R., III; Zhu, N-Z.; Russell, D. H.; Castro, M. E. *Proc. Natl. Acad. Sci. U.S.A.* 1987, 84, 620-23.
- (77) Shomo, R. E., II; Delmore, J. E.; Apelhans, A. D.; Dahl, D. A.; Marshall, A. G. *Proceedings of the 36th American Society for Mass Spectrometry Conference on Mass Spectrometry & Applied Topics*; San Francisco, CA, June 1988; pp. 1217-18.
- (78) Ipeza, I.; Knoll, H.; Wanzenk, K.-P.; Linden, H. B. *Proceedings of the 36th American Society for Mass Spectrometry Conference on Mass Spectrometry & Applied Topics*; San Francisco, CA, June 1988; pp. 1217-18.
- Lied Topics*; San Francisco, CA, June, 1988; pp. 618-19.
- (79) Loo, J. A.; Williams, E. R.; Amster, I. J.; Furlong, J. J. P.; Wang, B. H.; McLafferty, F. W.; Chait, B. T.; Field, F. H. *Anal. Chem.* 1987, 59, 1882-84.
- (80) Henry, K. D.; Williams, E. R.; Wang, B. H.; McLafferty, F. W.; Shabanowitz, J.; Hunt, D. F. *Proc. Natl. Acad. Sci. U.S.A.* 1989, 86, 9075-78.
- (81) Kofel, P.; McMahon, T. B. *Int. J. Mass Spectrom. Ion Proc.* 1990, 98, 1-24.

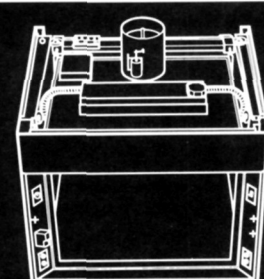
Chemistry Award in Chemical Instrumentation, the Eastern Analytical Symposium Award, the ACS Akron Section Award, and his election to the rank of fellow in both the American Physical Society and the American Association for the Advancement of Science.



Alan G. Marshall received his Ph.D. in physical chemistry from Stanford University in 1970. He joined the faculty at the University of British Columbia (Vancouver, Canada) in 1969 and moved to The Ohio State University in 1980 as professor of chemistry and biochemistry and director of the Chemical Instrument Center. He is best known for his co-invention (with M. B. Comisarow) and continuing development of FT-ICRMS, recognized by the ACS Division of Analytical



Peter B. Grosshans received his B.S. degree from the University of Colorado, Boulder, in 1983. He won an OSU Presidential Graduate Fellowship on the way to obtaining his Ph.D. in chemical physics in June 1990. Currently he is a postdoctoral fellow with Alan Marshall, who was also his graduate adviser. His research concerns the physics behind the FT-ICR technique; most notably, he is trying to linearize excitation and detection events simultaneously to make quantitative data accurate.



Well Built, Efficient, Safe, Cost Effective & Designed for Use

Fume hoods

New-TECH hoods provide the safety you require and the quality you desire. After all, they're built for **you**. We put years of fume hood sales/manufacturing experience together to develop just the right hood for you.

- Quality Craftsmanship
- Economical Cost Effectiveness

Fume hood control systems

You can reduce your lab utility expense drastically using our **fume hood control system with pneumatic powered door**. Is your lab frequently too hot or cold and do you find your hood sashes left open, in unsafe positions? If so, you are likely spending an extra \$4,000 to \$6,000 per each hood for your yearly heating and cooling!

- Immediate response, unlike most other sensing systems, increasing safety!
- Allows heating and cooling systems to operate under less dramatic demands, producing a more controlled and comfortable laboratory environment!
- Retrofits to most other competitors fume hood designs.



NEW-TECH

DISTRIBUTED BY TRI CITY LABORATORY SPECIALISTS

P.O. Box 1944 Midland, MI 48641-1944 (517) 496-2994 FAX (517) 496-2811

CIRCLE 136 ON READER SERVICE CARD